LCC-0142
SLAC-PUB-10592
July 2004

Linear Collider Collaboration Tech Notes

Compensation of Detector Solenoid Effects on the Beam Size in Linear Collider

Yuri Nosochkov and Andrei Seryi

Stanford Linear Accelerator Center
Stanford University
2575 Sand Hill Road
Menlo Park, CA

Abstract: In this paper, we discuss the optics effects of the realistic detector solenoid field on beam size at the Interaction Point (IP) of a future Linear Collider and their compensation. It is shown that most of the adverse effects on the IP beam size arise only from the part of the solenoid field which overlaps and extends beyond the final focusing quadrupoles. It is demonstrated that the most efficient and local compensation can be achieved using *weak antisolenoids* near the IP, while a correction scheme which employs only skew quadrupoles is less efficient, and compensation with strong antisolenoids is not appropriate. One of the advantages of the proposed antisolenoid scheme is that this compensation works well over a large range of the beam energy.

Work supported by Department of Energy contract DE-AC03-76SF00515.

Compensation of Detector Solenoid Effects on the Beam Size in Linear Collider

Yuri Nosochkov and Andrei Seryi
Stanford Linear Accelerator Center, P.O.Box 20450, Stanford, CA 94309
(Dated: July 28, 2004)

In this paper, we discuss the optics effects of the realistic detector solenoid field on beam size at the Interaction Point (IP) of a future Linear Collider and their compensation. It is shown that most of the adverse effects on the IP beam size arise only from the part of the solenoid field which overlaps and extends beyond the final focusing quadrupoles. It is demonstrated that the most efficient and local compensation can be achieved using *weak antisolenoids* near the IP, while a correction scheme which employs only skew quadrupoles is less efficient, and compensation with strong antisolenoids is not appropriate. One of the advantages of the proposed antisolenoid scheme is that this compensation works well over a large range of the beam energy.

PACS numbers: 29.17.+w, 41.85.-p, 41.75.Ht, 29.27.-a, 29.27.Hj, 84.71.Ba

I. INTRODUCTION

A Linear Collider (LC) must collide nanometer scale flat beams at the Interaction Point (IP) in order to reach the desired luminosity. The LC beam sizes are typically several nanometers in vertical and several hundred nanometers in horizontal plane. To produce these very small beam sizes requires strong optics and careful attention to any effects that can degrade the ideal beam, and in particular, compensating the coupling and other distortions introduced by the detector solenoid.

In circular colliders, the standard methods of compensating for the detector solenoid include antisolenoids or skew quadrupoles or their combination. The simplest correction employs a pair of antisolenoids installed on either side of the detector solenoid. In this scheme of *strong antisolenoids*, the combined strength of the compensating and detector solenoids on each side of IP must vanish in order to cancel the beam tilt both at the IP and outside of the solenoid. This is automatically achieved if there are no other magnets inside the solenoid. The advantage of this scheme is that it is completely local and corrects all energies at once, but the drawback is that the antisolenoids do not permit the Interaction Region (IR) quadrupoles to be placed close to the IP. This limits the strength of the final beam focusing and hence the luminosity. This type of compensation was used in the early SPEAR and PEP [1] colliders and is presently used at KEK-B [2].

The *strong antisolenoid* method can be expanded to include quadrupoles inside the solenoid field. In this case, each quadrupole inside the field must be rotated by the same angle as the coupled beam would have at that quadrupole location. The tilted quadrupoles do not generate additional coupling, and hence the solenoid-antisolenoid compensation is preserved. For ideal correction, however, the quadrupole frame would have to rotate continuously along the quadrupole length to follow the beam angle. For practical purposes, the continuous rotation can be replaced by an average tilt angle in each quadrupole and the remaining residual coupling minimized by small adjustment of the tilt angles as is done at DAFNE [3]. One disadvantage of this scheme is that operating at a different energy or different solenoid field requires a mechanical adjustment of the quadrupole tilt which may be technically difficult.

Solenoid compensation using only skew quadrupoles has been implemented, for example, at the e^+e^- colliders LEP [4] and PEP-II [5]. In this scheme, local compensation of the coupling terms at the IP requires up to four skew quadrupoles on each side of the IP. The number of correctors may be reduced if the optics is symmetric about the IP or if some coupling terms can be neglected. Advantages of this method are that the skew quadrupoles are shorter than the antisolenoids, do not require space near the IP, can be adjusted for changing optics parameters, and can correct coupling coming from other sources. The drawback is that this correction, typically, is not as local as the *strong antisolenoid* scheme because the skew quadrupoles have to be placed at locations with specific phase advance from the IP. Consequently, the longer correction region in the real machine includes more magnet errors and, hence, requires a more careful implementation.

Compared to circular machines, the solenoid compensation in linear colliders has a few distinctive features: 1) correction is essential up to the collision point but may not be so stringent afterwards; 2) the IP beam focusing is much stronger than in existing rings; and 3) the optics must accommodate a large range of beam energy. For example in the next generation Linear Collider, the IP must be designed to cover 90 GeV to 1 TeV in the center of mass. The standard methods of solenoid compensation used in circular accelerators are not appropriate for a linear collider. A novel method of *weak antisolenoids* appears to be the optimal compensation strategy.

This paper evaluates the effects of the detector solenoid field on the beam size and orbit at the IP of the Next Linear Collider (NLC). The study assumes the design optics of the NLC Beam Delivery System (BDS) with realistic models of the detector solenoid field, provides both the analytical estimate and particle tracking calculation of

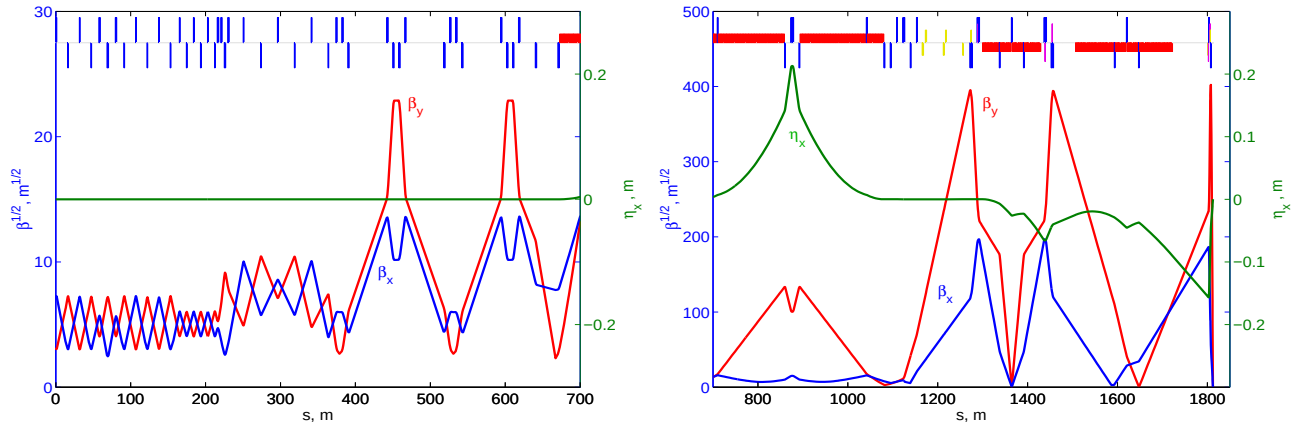

FIG. 1: Optics of the NLC Beam Delivery System. The IP is located at s=1812.56 m. A skew correction section is located in the first hundred meters. Correction sextupoles, whose displacements form the linear knobs, are at maxima of the beta function near s=1270 and 1450 m and in the FD.

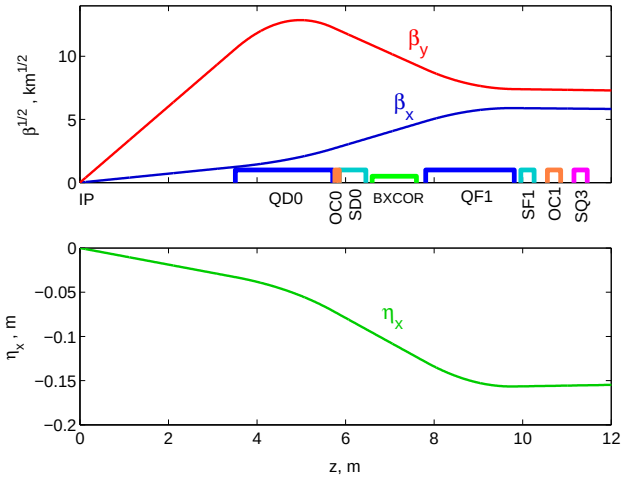

FIG. 2: Optics of the Next Linear Collider Beam Delivery System near the Interaction Point showing betatron functions (top plot) and horizontal dispersion (bottom plot). Locations of the Final Doublet magnets are shown, including quadrupoles QD0 and QF1, sextupoles SD0 and SF1, octupoles OC0 and OC1, skew quadrupole SQ3 and optional vertical corrector BXCOR.

the effects on the beam, and discusses possible methods of compensation.

All presented calculations are for the optics of the first Interaction Region in the NLC design [6] and for a beam energy of 250 GeV. The ideal rms beam sizes at the IP are $\sigma_{x0} = 243$ nm and $\sigma_{y0} = 3$ nm, and beam divergencies $\sigma_{xp0} = 30.4$ μrad and $\sigma_{yp0} = 27.3$ μrad. The energy spread has a "Batman" two-horn distribution with the half width of 0.4 % (corresponding to the effective rms value of $\sigma_E \approx 0.25$ %). The IP beta functions are $\beta_{x0} = 8$ mm, $\beta_{y0} = 0.11$ mm, and there is a nonzero horizontal angular dispersion $\eta'_{x0} = 0.0094$ at the IP. The latter is needed to create dispersion at the Final Doublet sextupoles for a local correction of the BDS chromaticity [7]. The optics of the complete BDS is shown in Fig. 1 and the optics near the IP is shown in Fig. 2. The free space between the IP and the Final Doublet is $L_* = 3.51$ m, and the half crossing angle is $\theta_c = 10$ mrad. These figures also show the locations of the Final Doublet (FD) quadrupoles, correcting sextupoles, octupoles and skew quadrupole near the IP, and the location of the skew correction section and sextupoles forming the linear knobs in the BDS.

Two realistic detector solenoid models were considered: the Silicon Detector (SiD) and the Large Detector (LD). The maximum field values are 5 T and 3 T, respectively, and the corresponding field integrals over half the detector are 16.7 Tm and 14.4 Tm. Figures 3 and 4 show the ANSYS models for these detectors and the calculated longitudinal and radial components of the solenoid field.

For comparison with the above realistic models, a fictitious "tiny" solenoid model was also studied. This model was scaled from SiD and compressed longitudinally with the maximum field of 12 T and the field integral over half the detector of 18.0 Tm as shown in Fig. 5. The essential feature of this model is that the solenoid is chosen to be short enough so that it does not overlap with the Final Doublet, in contrast to SiD or LD models.

The organization of this paper is as follows: Section II recapitulates the optics transformation in the basic hard edge solenoid model. Section III introduces the effects generated in the realistic solenoid models with overlapping solenoid field and Final Doublet quadrupoles. Section IV provides an analytic description of the coupling and orbit effects at the IP due to the overlapped quadrupoles. The results of tracking simulations are presented in Section V along with optimized configurations of the antisolenoids for the SiD and LD models and the compensation results. The enhancement of the effects at lower beam energies, and performance of compensation using the weak antisolenoid in comparison with skew quadrupole compensation method are discussed in Section V as well.

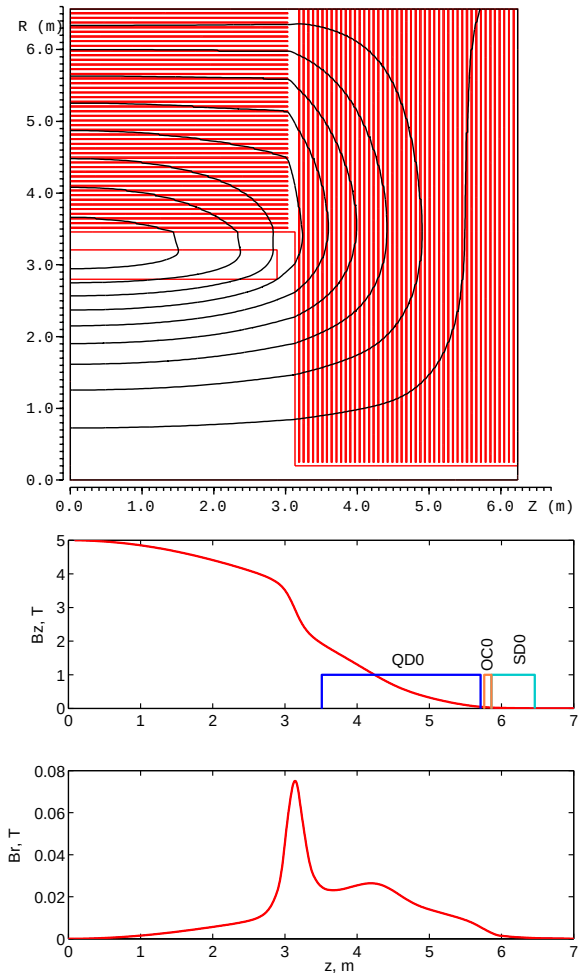

FIG. 3: The model of the Silicon Detector (SiD) with field lines calculated by ANSYS (top plot). Longitudinal and radial fields on the ideal beam trajectory with half crossing angle $\theta_c = 10$ mrad (bottom plots). Locations of the Final Doublet elements are also shown. IP is at $z = 0$ m.

II. HARD EDGE SOLENOID MODEL

Let us first describe the well-known properties of a simple hard edge solenoid with constant longitudinal field B and length ℓ. The first order matrix in this model can be written as $\hat{M}_S = \hat{M}_E\ \hat{M}_L\ \hat{M}_E{}^{-1}$, where matrices $\hat{M}_E$ and $\hat{M}_E{}^{-1}$ represent the integral effect of a linear radial field at the two solenoid edges and $\hat{M}_L$ is the transformation produced by the longitudinal field in the solenoid body (see for example [8]):

$$\hat{M}_E = \begin{pmatrix} 1 & 0 & 0 & 0 \\ 0 & 1 & -K_S & 0 \\ 0 & 0 & 1 & 0 \\ K_S & 0 & 0 & 1 \end{pmatrix}, \qquad (1)$$

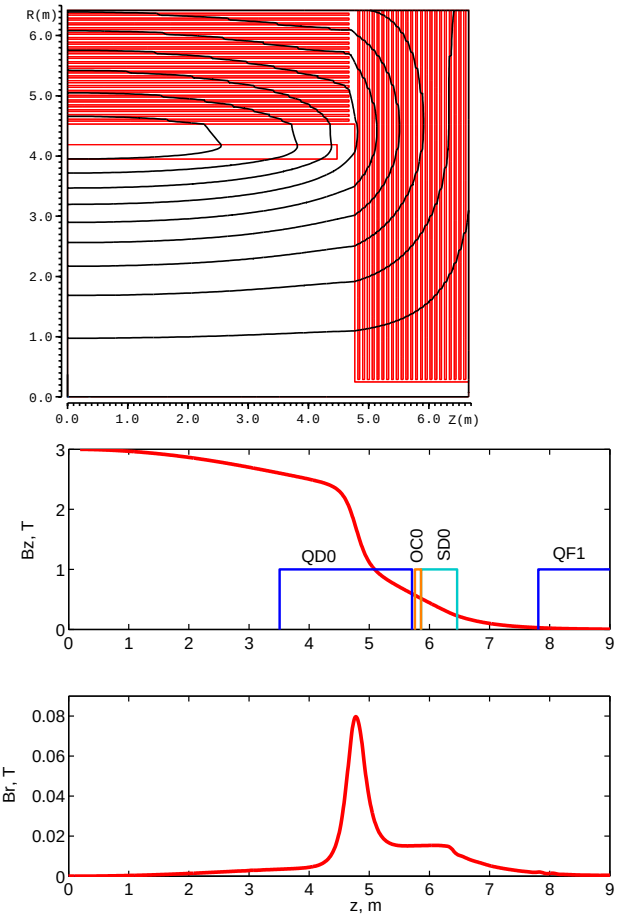

FIG. 4: The model of the Large Detector (LD) with field lines calculated by ANSYS (top plot). Longitudinal and radial fields on the ideal beam trajectory with half crossing angle $\theta_c = 10$ mrad (bottom plots). Locations of the Final Doublet elements are also shown. IP is at $z = 0$ m.

$$\hat{M}_L = \begin{pmatrix} 1 & SC/K_S & 0 & S^2/K_S \\ 0 & C^2 - S^2 & 0 & 2SC \\ 0 & -S^2/K_S & 1 & SC/K_S \\ 0 & -2SC & 0 & C^2 - S^2 \end{pmatrix}, \qquad (2)$$

$$\hat{M}_S = \begin{pmatrix} C^2 & SC/K_S & SC & S^2/K_S \\ -SCK_S & C^2 & -S^2K_S & SC \\ -SC & -S^2/K_S & C^2 & CS/K_S \\ S^2K_S & -SC & -SCK_S & C^2 \end{pmatrix}. \qquad (3)$$

Here, $K_S = B/(2B\rho)$, $S = \sin K_S\ell$, $C = \cos K_S\ell$, and $B\rho$ is the magnetic rigidity (equal to about 834 Tm at 250 GeV). Note that the full solenoid matrix $\hat{M}_S$ is symplectic, but the individual matrices $\hat{M}_E$ and $\hat{M}_L$ do not satisfy this condition. This is because the matrices are written in terms of TRANSPORT variables (x, x', y, y'), while the symplecticity condition is derived and satisfied in the canonical system (x, p_x, y, p_y). The two sets of variables are equal in a purely transverse field, hence the matrices of such magnets are automatically symplectic in

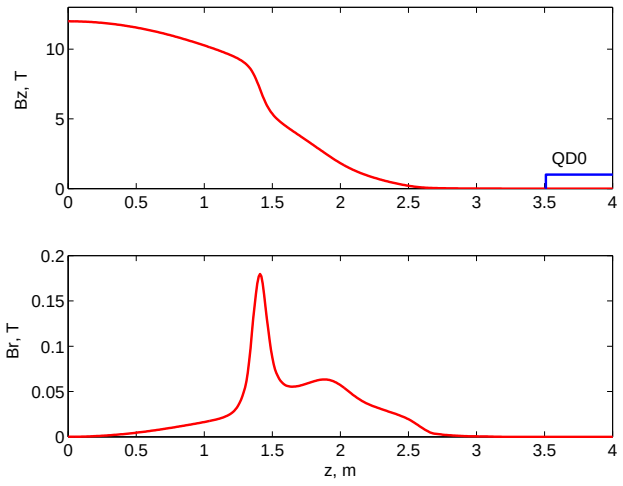

FIG. 5: Fields of fictitious "tiny" detector. Longitudinal and radial fields on the ideal beam trajectory with half crossing angle $\theta_c = 10$ mrad. Locations of the Final Doublet elements are also shown. IP is at $z = 0$ m.

a (x, x', y, y') system. Inside a solenoid, however, there is a difference between the mechanical (x', y') and canonical (p_x, p_y) momenta created by the non-zero transverse components of the magnetic vector potential of a longitudinal field. Since the canonical transformation remains symplectic by definition, the transformation of (x, x', y, y') inside a solenoid is no longer symplectic. This deviation arises only while inside a solenoid and should not be a concern [9].

Analysis of Eqn. 3 shows that $\hat{M}_S$ can be expressed in a simpler form using a symplectic 2×2 matrix $\hat{F}$:

$$\hat{M}_S = \begin{pmatrix} C\hat{F} & S\hat{F} \\ -S\hat{F} & C\hat{F} \end{pmatrix}, \text{where } \hat{F} = \begin{pmatrix} C & S/K_S \\ -SK_S & C \end{pmatrix}. \quad (4)$$

From here, it follows that $\hat{M}_S$ can be written as a product of an uncoupled matrix $\hat{M}_F$ and a rotation matrix $\hat{M}_R$, both being symplectic:

$$\hat{M}_S = \hat{M}_F\,\hat{M}_R = \hat{M}_R\,\hat{M}_F, \quad (5)$$

$$\hat{M}_F = \begin{pmatrix} \hat{F} & \hat{O} \\ \hat{O} & \hat{F} \end{pmatrix}, \ \hat{M}_R = \begin{pmatrix} C\hat{I} & S\hat{I} \\ -S\hat{I} & C\hat{I} \end{pmatrix}, \quad (6)$$

$$\text{where } \hat{I} = \begin{pmatrix} 1 & 0 \\ 0 & 1 \end{pmatrix}, \ \hat{O} = \begin{pmatrix} 0 & 0 \\ 0 & 0 \end{pmatrix}. \quad (7)$$

Eqns. 5, 6 clearly show that the solenoid coupling is just a rotation of the beam envelope in the $x-y$ plane by the angle $K_S\ell = B\ell/(2B\rho)$. The uncoupled matrix $\hat{M}_F$ provides equal transformation in x and y planes. In the approximation that the solenoid field is weak with $K_S\ell \ll 1$ (typically true for detector solenoids in accelerators), the $\hat{M}_F$ can be represented by a thin focusing lens surrounded by drifts of length $\ell/2$:

$$\hat{M}_F = \begin{pmatrix} 1 & \frac{\ell}{2} & 0 & 0 \\ 0 & 1 & 0 & 0 \\ 0 & 0 & 1 & \frac{\ell}{2} \\ 0 & 0 & 0 & 1 \end{pmatrix} \begin{pmatrix} 1 & 0 & 0 & 0 \\ -K_S^2\ell & 1 & 0 & 0 \\ 0 & 0 & 1 & 0 \\ 0 & 0 & -K_S^2\ell & 1 \end{pmatrix} \begin{pmatrix} 1 & \frac{\ell}{2} & 0 & 0 \\ 0 & 1 & 0 & 0 \\ 0 & 0 & 1 & \frac{\ell}{2} \\ 0 & 0 & 0 & 1 \end{pmatrix}, \quad (8)$$

where the focusing terms $-K_S^2\ell$ are equal in the x and y planes. Finally, taking into account that the rotation and drift matrices commute, a weak solenoid of length ℓ can be approximated by a thin solenoid with the matrix containing only the focusing and rotation terms as follows [8]:

$$\hat{M}_S^{\,thin} = \begin{pmatrix} 1 & 0 & K_S\ell & 0 \\ -K_S^2\ell & 1 & 0 & K_S\ell \\ -K_S\ell & 0 & 1 & 0 \\ 0 & -K_S\ell & -K_S^2\ell & 1 \end{pmatrix}, \quad (9)$$

and drifts of length $\ell/2$ on either side. Note that in this approximation, $\hat{M}_S^{\,thin}$ is symplectic only to the first order of $K_S\ell$.

III. SOLENOID EFFECTS WITH REALISTIC MODELS

The situation becomes much more complicated for realistic models of the detector solenoid. The solenoid field is not constant along the longitudinal axis, the fringe field extends well inside the FD quadrupoles, and the solenoid is horizontally tilted with respect to the beam trajectory. Because preservation of the small vertical beam size at the IP is so essential for any linear collider, the most important effects to be identified and compensated are those that affect the vertical beam size.

The following discussions will often use the projection method [10], where beam aberrations originating at various locations in the lattice, for example in the solenoid, are projected to the IP by an appropriate optics transformation. The projected aberrations can be expressed in the form of matrix terms at the IP which add linearly, thus simplifying the analysis of their effects on the IP beam size.

Based on Eqns. 5, 6, the beam rotation in a solenoid field is equivalent to a $\langle yx\rangle$ coupling at the IP ($\langle 31\rangle$ matrix term) equal to $\approx B\ell/(2B\rho)$ which is on the order of 1% in NLC for 250 GeV. Consequently, the IP vertical beam size would increase as $\frac{\sigma_y}{\sigma_{y0}} \approx \sqrt{1+(\frac{\sigma_{x0}}{\sigma_{y0}}\frac{B\ell}{2B\rho})^2}$ yielding less than a factor of two of beam size growth at the IP. It was also shown in Refs. [11–13] and can be verified using Eqn. 9 that the geometric and chromatic orbit displacements generated when the beam passes through the solenoid at an angle are cancelled at the IP as long as

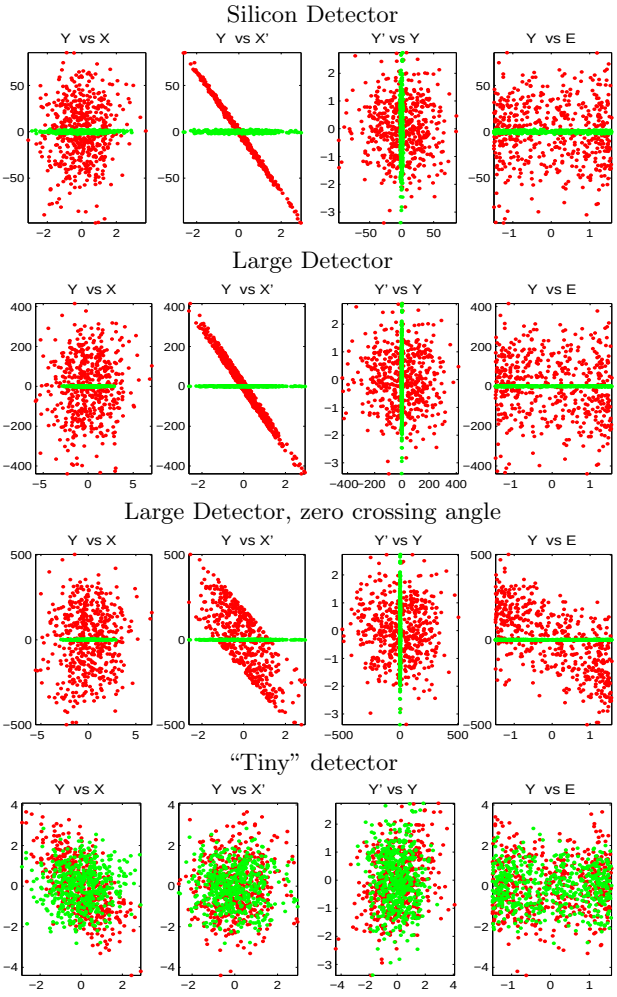

FIG. 6: Beam phase space at the IP obtained by tracking with four different detector solenoid models. Green dots show the ideal beam (no detector field), red – with detector solenoid field. Coordinates are normalized to the ideal beam sizes. No correction of the beam size was applied.

the collision point is located on the solenoid axis and the typically small transverse focusing due to the solenoid is neglected. For example, the vertical orbit deviates from the zero plane at the entrance to and along the solenoid, but returns exactly to zero at the IP in this approximation. This cancellation results from the fact that the solenoid radial and longitudinal fields have opposite effects on the beam orbit.

The above estimate, however, is only correct if there are no other magnets inside the solenoid (such as in the "tiny" model). Effects generated by the solenoid field extending into the final focus quadrupoles have been evaluated in several studies using numeric calculations with optics and tracking codes (see for example [5, 13–16]). It was noted that the overlap of the solenoid and quadrupole fields gives rise to new coupling terms at the IP and significantly increases the vertical beam size. In particular, the $\langle yx' \rangle$ correlation term at the IP [14] was

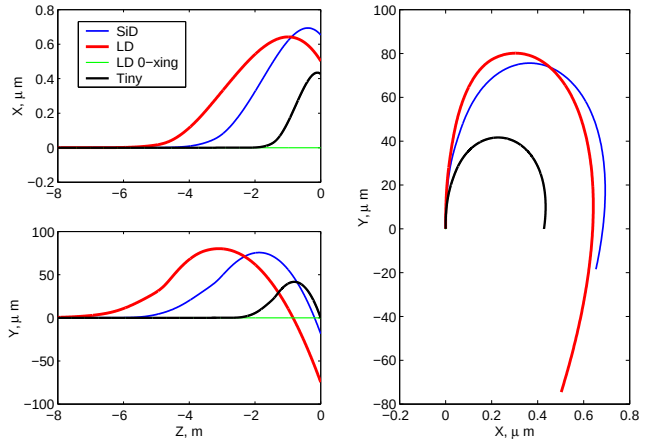

FIG. 7: Beam orbits obtained by tracking with four different solenoid models. IP is at $z = 0$ m.

observed to cause large beam size growth at SLC.

Tracking results for the realistic NLC detector solenoid models are presented in Fig. 6 which shows the beam phase space at the IP obtained using the DIMAD code [17], for four cases (SiD, LD, "tiny" detector and LD with zero crossing angle). One can see that the vertical beam size growth is indeed about a factor of 2 for the "tiny" detector, but it is almost two orders of magnitude larger in the other three cases where the solenoid field extends into the FD quadrupoles. One can see in Fig. 6 that the main contribution to the IP beam size is produced not by the $\langle yx \rangle$ term, but by $\langle yx' \rangle$ coupling when the solenoid and quadrupoles overlap. Additionally, as shown in Fig. 7, there is a non-zero vertical displacement of the beam at the IP. A quadrupole inserted inside the solenoid breaks the natural compensation of the IP orbit produced by the solenoid radial and longitudinal fields.

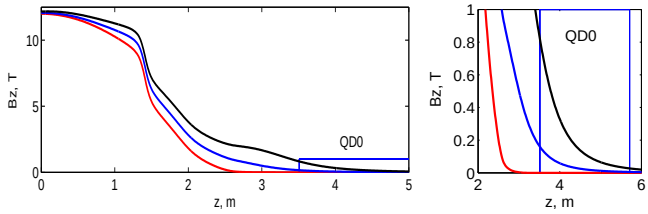

FIG. 8: Tiny detector with small additional field giving 0.1 Tm or 0.5 Tm integrated over FD (indicated as "Tiny $+\Delta_1$" and "Tiny $+\Delta_2$" in the Table I).

A more systematic illustration of the effect of the solenoid and quadrupole overlap is presented in Figures 8 and 9, where the solenoid field integral of the "tiny" detector is increased in two steps in order to add a small part of the field (0.1 and 0.5 Tm) on top of the FD quadrupole. One can see that even a relatively small amount of solenoid field in the quadrupole significantly increases the coupling and beam size at IP.

Solenoid effects for different detector field models are summarized in Table I. It is clear that the major effect

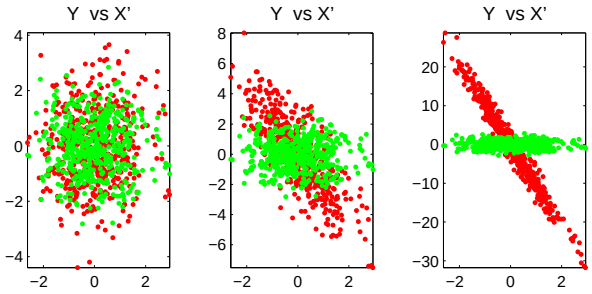

FIG. 9: Beam phase space at the IP in the "Tiny" detector without (left plot) and with small additional field (middle plot – "Tiny $+\Delta_1$", right – "Tiny $+\Delta_2$").

TABLE I: Uncompensated solenoid effects on the 250 GeV beam for different NLC detector models. Here $B\ell$ is the full field integral over half the detector, and $B\ell_{FD}$ is its fraction over the Final Doublet, i.e. for $z > 3.51$ m. The correlation terms $\langle yx' \rangle$ and $\langle yE \rangle$ are normalized to the nominal rms beam sizes.

Detector	$B\ell$ Tm	$B\ell_{FD}$ Tm	y_{IP} μm	σ_x/σ_{x0}	σ_y/σ_{y0}	$\langle yx' \rangle$	$\langle yE \rangle$
SiD	16.7	1.7	-18.5	1.1	31.5	-32.8	-0.33
LD	14.4	4.4	-74.5	2.2	149.2	-153.4	-18.0
LD, 0-xing	14.4	4.4	0	2.1	187.1	-141.1	-122.9
"Tiny"	18.0	0	0	1.0	1.31	0.0	0.0
Tiny $+\Delta_1$	20.2	0.1	-1.05	1.0	2.34	-2.00	-0.15
Tiny $+\Delta_2$	22.1	0.5	-5.22	1.03	10.5	-10.51	-0.98

on the IP beam size comes from that part of the solenoid that overlaps with the Final Doublet. On the contrary, if the solenoid field does not enter the quadrupoles, there is a natural cancellation of the solenoid induced orbit at the IP and, to a major extent, suppression of the beam size growth. Table I also shows that a non-zero crossing angle does not significantly alter the uncompensated beam size (comparing the two LD cases).

In the IR designs for TESLA and NLC, the FD quadrupoles are placed inside the detector solenoid field. Earlier studies of solenoid compensation for these projects used skew quadrupole correction [13, 15, 16]. For both NLC and TESLA, a skew quadrupole placed at the Final Doublet removed most of coupling generated by the overlapped quadrupoles. By adding a second skew quadrupole or using a skew correction section and compensating the beam waist position, the IP beam size could be brought close to design. However, in this scheme the skew quadrupoles have to become stronger for lower beam energies.

Naturally, it is desirable to compensate the coupling effects of an overlapped quadrupole at its source, i.e. at the quadrupole, thus restoring the properties of a bare solenoid. In this paper, we discuss such a method of compensation in the Linear Collider IR using *weak antisolenoids* overlapping with the Final Doublet. An important feature of this scheme is that the weak antisolenoids do not need to compensate the entire field of the detector solenoid, but only the much smaller part which overlaps with the Final Doublet.

As will be shown below, compensation with weak antisolenoids is superior that with skew quadrupoles, and it is effective over the entire NLC energy range from 50 to 250 GeV/beam. It is also insensitive to changes of the beam optics, and compatible with compensation of the vertical orbit angle at the IP [18].

IV. ANALYTIC DESCRIPTION OF EFFECTS OF SOLENOID OVERLAPPING WITH FINAL DOUBLET

To investigate analytically the effect of the solenoid on the NLC beam, it is useful to consider a short test solenoid with field integral $B\ell = 0.5$ Tm, placed at various positions near the IP, instead of the full detector solenoid. The overall effect of a realistic solenoid field can then be evaluated by integration.

Two cases are discussed: 1) the test solenoid is coaxial with the detector, and 2) the test solenoid is coaxial with the beam, analogous to the possible configurations of the weak compensating antisolenoid discussed in Section V that can be built-in into the detector or wound on a final quadrupole. In both these cases, the incoming beam travels at an angle to the detector axis equal to half of the NLC crossing angle θ_c. The difference between the two cases is the radial field seen by the beam at the entrance to the test solenoid. In the first case, this field is not zero since the incoming beam is horizontally offset with respect to the solenoid axis. In the second case, there is no radial field on the beam axis.

The derivations presented in this Section are performed in the approximation of a weak solenoid and assumption that solenoid transverse focusing can be neglected, in particular, that the unperturbed design twiss functions of BDS can be used, and the effects of the solenoid focusing on the orbit are small. Validity of this assumption will be discussed later.

Let us first consider how the test solenoid placed on the detector axis affects the beam orbit. As follows from Eqn. 9, a thin solenoid located at distance Z_s from the IP and traversed at horizontal radius $-Z_s\ \theta_c$ and angle θ_c will cause the vertical orbit and angle to change by

$$\Delta y\ =\ \frac{B\ell\ Z_s\ \theta_c}{2B\rho} \qquad \text{and} \qquad \Delta y'\ =\ -\frac{B\ell\ \theta_c}{2B\rho}. \quad (10)$$

Clearly, if there are no focusing elements between the solenoid and the IP, then the vertical offset at the IP will exactly cancel since $y_{IP} = \Delta y + Z_s \Delta y' = 0$. If there is a quadrupole field after the solenoid, it focuses the orbit and breaks the cancellation. Note that the IP orbit angle produced by solenoid does not cancel.

An example of the orbit created by the test solenoid located at $Z_s = 10$ m is shown in Fig. 10. Here the or-

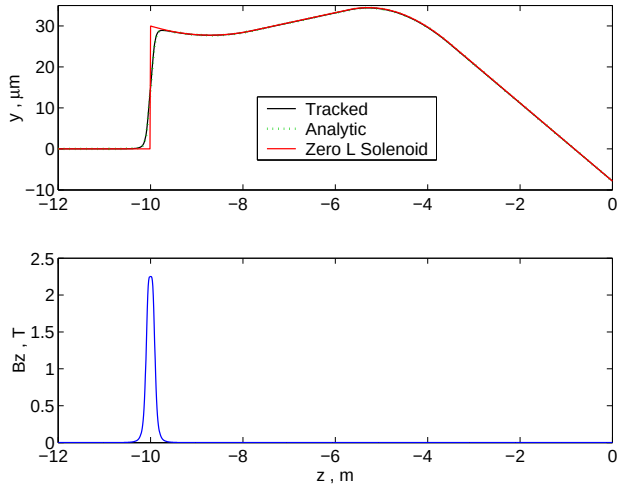

FIG. 10: Orbits with a short test solenoid of $B\ell$=0.5 Tm placed *on the detector axis* at 10 m from the NLC IP. Orbits are obtained using particle tracking and analytical integration of the field for the exact model, and with a zero length approximation of the solenoid. IP is at $z = 0$ m.

bit obtained by tracking in DIMAD is compared with an analytic calculation integrating the horizontal field B_x of the solenoid and FD quadrupoles (including the additional case of a very thin solenoid with $\ell \to 0$):

$$\frac{d^2y}{dz^2} = \frac{B_x}{B\rho} + \frac{G(z)\,y}{B\rho}, \qquad (11)$$

where $G(z)$ is the gradient of the FD quadrupoles. One can see that the thin solenoid approximation is in a good agreement with the calculation of the exact model using analytic and tracking methods. In DIMAD tracking, the FD region was modeled by a sequence of short, typically 1 cm long slices containing all the solenoid, dipole, quadrupole, sextupole and octupole fields, using the realistic solenoid field map and the design BDS optics.

Using the formalism of beam transport matrices, the orbit at the IP can be expressed as

$$\begin{aligned} y_{IP} &= \Delta y\, m_{33} + \Delta y'\, m_{34} \quad , \\ y'_{IP} &= \Delta y\, m_{43} + \Delta y'\, m_{44} \quad . \end{aligned} \qquad (12)$$

Here m_{ij} are elements of the transport matrix M from the test solenoid to the IP. Substituting the well-known twiss expressions for the matrix terms, the formula for y_{IP} can be written as

$$y_{IP} = \frac{B\ell\theta_c}{2B\rho}\sqrt{\beta_{y0}/\beta_y}(Z_sC_Y + Z_s\alpha_yS_Y - \beta_yS_Y), \qquad (13)$$

where $C_X = cos(\mu_x)$, $S_X = sin(\mu_x)$, $C_Y = cos(\mu_y)$ and $S_Y = sin(\mu_y)$ are functions of the horizontal and vertical phase advance $\mu_{x,y}$ between the test solenoid and the IP. β and α are the twiss parameters at the location of the test solenoid, and β_0 and $\alpha_0 = 0$ are the twiss parameters at IP, for the corresponding planes. Taking into account the analytic expressions for β, α and μ, one can verify that in the final drift before the IP

$$Z_sC_Y + Z_s\alpha_yS_Y - \beta_yS_Y = 0, \qquad (14)$$

and hence y_{IP} is exactly cancelled if there is only a drift between the test solenoid and the IP. Note that in Eqn. 14 the terms which mutually cancel are very large, of the order of L_*^2/β_{y0}, where L_* is the length of the final drift. If the test solenoid overlaps the FD quadrupoles, the sine terms become dominant, and the maximum offset at the IP can be estimated roughly as

$$y_{IP} \approx \frac{B\ell\,\theta_c}{B\rho}\,L_* \quad . \qquad (15)$$

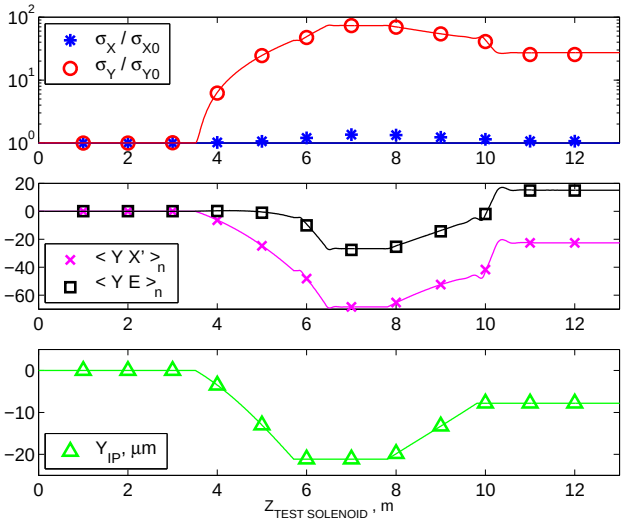

FIG. 11: Beam size, major correlations, and Y position at the IP for the short test solenoid placed *on the detector axis*. Symbols – tracking, solid line – analytic solutions. IP is at $z = 0$ m.

The effect of the test solenoid on the beam offset at the IP is shown in Fig. 11 (the lower plot), where one can see the perfect orbit cancellation in the last drift and good agreement between tracking and analytical results obtained using Eq. 13.

Now let us consider the effect of the solenoid on the dominant IP aberration terms – the coupling $\langle yx'\rangle$ and dispersion $\langle yE\rangle$. Figures 11 and 12 show these terms and the beam size growth at the IP as a function of the test solenoid position, where the tracking results are compared with analytical values given by the expressions derived below.

If the test solenoid is placed on the beam axis, the projected coupling term $\langle yx'\rangle$ does not depend on the crossing angle and is given by (normalized to the nominal rms beam sizes):

$$\langle yx'\rangle_{\theta=0} = \frac{\sigma_{xp0}}{\sigma_{y0}}\,\frac{B\ell}{2\,B\rho}\,(m_{12}m_{33} - m_{11}m_{34}). \qquad (16)$$

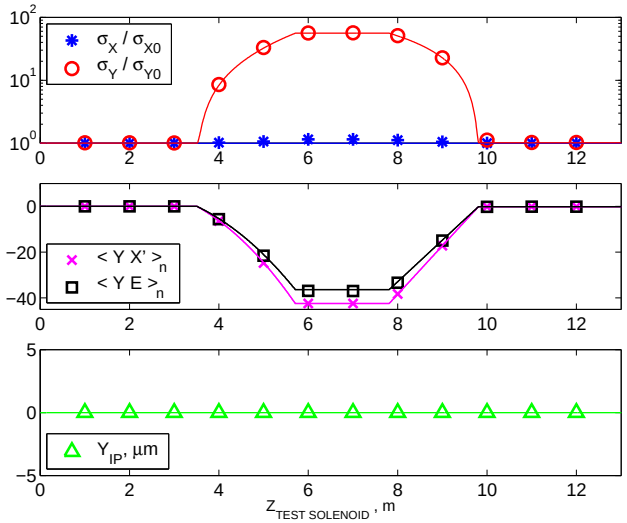

FIG. 12: Beam size, major correlations, and Y position at the IP for the short test solenoid placed *on the beam axis*. Symbols – tracking, solid line – analytic solutions. IP is at $z = 0$ m.

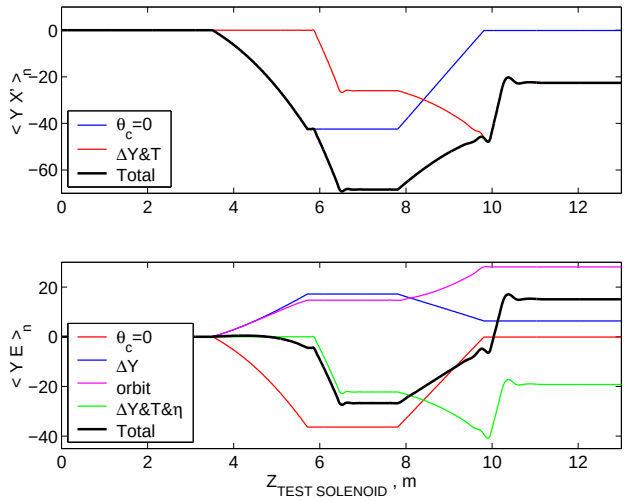

FIG. 13: Contributions of different terms to the coupling $\langle yx' \rangle$ and vertical dispersion $\langle yE \rangle$ for the test solenoid placed *on the detector axis*, based on analytic calculation. Coupling (top plot) includes a term independent of crossing angle (blue line) and a term from the orbit kicks and the second order matrix (red line). Dispersion (bottom plot) includes contribution from the angle independent coupling (red line), and three additional terms due to the energy dependence of the kicks (blue line), to the vertical offset in the quadrupoles (magenta line), and to the second order matrix, horizontal dispersion and orbit kick (green line).

This equation is derived by taking into account that the solenoid matrix M_S projected to IP [10] is:

$$M_{Sproj} = M \;\; M_S \;\; M^{-1} \;\; . \tag{17}$$

Expanding Eqn. 16 in terms of twiss parameters, we obtain

$$\langle yx' \rangle_{\theta=0} \;=\; \frac{\sigma_{xp0}}{\sigma_{y0}} \, \frac{B\ell}{2\,B\rho} \, \frac{\sqrt{\beta_{x0}\beta_{y0}}}{\sqrt{\beta_x \beta_y}} \tag{18}$$
$$\times (\alpha_y \beta_x S_X S_Y + \beta_x S_X C_Y - \beta_y S_Y C_X - \alpha_x \beta_y S_X S_Y) \; .$$

The terms in the parenthesis are very large, of the order of $L_*^3/(\beta_{x0}\beta_{y0})$, however they again cancel exactly in the last drift. The latter is easy to see applying $m_{11} = m_{33} = 1$ and $m_{12} = m_{34} = Z_s$ in Eqn. 16, or using Eq. 14. Another case of exact cancellation is the so called "parallel-to-point" transformation, where $m_{11} = m_{33} = 0$ which roughly represents the matrix from the drift prior to the Final Doublet where the beam is almost parallel. In general, cancellation of $\langle yx' \rangle$ in Eqn. 16 occurs for a symmetric x and y transformation with $m_{11} = m_{33}$ and $m_{12} = m_{34}$. This can also be concluded from Eqns. 5, 6 which show that a symmetric x-y matrix commutes with the solenoid rotation matrix, hence does not change the solenoid coupling.

Obviously, when the test solenoid is inside the Final Doublet, the opposite quadrupole focusing in two planes breaks the x and y symmetry and, hence, the cancellation of $\langle yx' \rangle$. Thus, one can conclude that the philosophical reason for the breakdown of the cancellation is that the FD quadrupoles affect two planes differently, i.e. defocus in one plane and focus in another.

The maximal effect of this coupling term, with the test solenoid in the FD, can be estimated as

$$\langle yx' \rangle_{\theta=0} \;\approx\; \frac{\sigma_{xp0}}{\sigma_{y0}} \, \frac{B\ell}{B\rho} \, L_* \quad . \tag{19}$$

We can see in Fig. 12 that agreement between tracking and the analytical formula is very good. It is also very interesting to note, from this Figure, that there is a very good cancellation also for the case when the test solenoid is placed after the Final Doublet. As we just discussed above, this happens because the beam after the final doublet is almost parallel in both planes. Equation 18 shows that in this case the cancellation is only approximate, since the location of the effective image points upstream of the FD for the x and y planes usually do not occur at the same location.

For the test solenoid placed on the beam axis, the vertical dispersion at the IP $\langle yE \rangle$ arises from the solenoid coupling of the horizontal dispersion into the vertical plane:

$$\langle yE \rangle_{\theta=0} \;=\; -\frac{\sigma_E}{\sigma_{y0}} \, \frac{B\ell}{2\,B\rho} \, (m_{33}\,\eta_x \;+\; m_{34}\,\eta_x') \; , \tag{20}$$

where η_x and η_x' are the horizontal dispersion and its derivative at the location of the test solenoid. Expanding, we obtain:

$$\langle yE \rangle_{\theta=0} \;=\; -\frac{\sigma_E}{\sigma_{y0}} \, \frac{B\ell}{2\,B\rho} \tag{21}$$
$$\times \left(\sqrt{\beta_{y0}/\beta_y} \, (C_Y + \alpha_y S_Y) \, \eta_x \;+\; \sqrt{\beta_{y0}\beta_y} \, S_Y \, \eta_x' \right) \; .$$

For the case where the angular horizontal dispersion is nominally nonzero at the IP, and the dispersion itself is zero, Eq. 20 can be rewritten as

$$\langle yE\rangle_{\theta=0} \;=\; \frac{\sigma_E}{\sigma_{y0}}\,\frac{B\ell}{2\,B\rho}\,\eta'_{x0}\,(m_{12}m_{33} \;-\; m_{11}m_{34})\;, \quad (22)$$

which has exactly the same dependence as the coupling term in Eq. 16. This means that both major correlations can be corrected simultaneously by the weak antisolenoid discussed in Section V.

Fig.12 shows that agreement between the simulations and these analytical expressions is good. Similarly as for Eq. 19, the approximation for the maximal effect on the vertical dispersion term can be written as

$$\langle yE\rangle_{\theta=0} \;\approx\; \frac{\sigma_E}{\sigma_{y0}}\,\frac{B\ell}{B\rho}\,\eta'_{x0}\,L_*\;. \quad (23)$$

Let us now derive the coupling and dispersion terms for the case when the test solenoid is placed on the detector axis. This case must include the kick on the orbit Δy and $\Delta y'$ at the location of the test solenoid as given by Eq. 10. Since these kicks are large, the second order transfer matrix T (its elements are t_{ijk}) from the test solenoid to the IP must also be taken into account.

Correspondingly, the $\langle yx'\rangle$ coupling will be given by

$$\langle yx'\rangle \;=\; \langle yx'\rangle_{\theta=0} \;+\; \frac{\sigma_{xp0}}{\sigma_{y0}} \quad (24)$$
$$\times\,(-(t_{331}\Delta y + t_{341}\Delta y')m_{12} + (t_{332}\Delta y + t_{342}\Delta y')m_{11})\;,$$

where the additional term is proportional to θ_c.

In the case of the test solenoid located on the detector axis, there are three additional terms which contribute to the vertical dispersion $\langle yE\rangle$. These are:
a) the term due to the energy dependence of the kicks Δy and $\Delta y'$:

$$\delta\,\langle yE\rangle \;=\; \frac{\sigma_E}{\sigma_{y0}}\,(-m_{33}\Delta y \;-\; m_{34}\Delta y') \;= \\ = \frac{\sigma_E}{\sigma_{y0}}\,\frac{B\ell}{2\,B\rho}\,(-m_{33}Z_s \;+\; m_{34})\,\theta_c\;; \quad (25)$$

b) the term due to the vertical orbit offset in the quadrupoles of the Final Doublet, which can be obtained by integration of the known orbit or, equivalently, by using the second order matrices:

$$\delta\,\langle yE\rangle \;=\; \frac{\sigma_E}{\sigma_{y0}}\,(t_{336}\Delta y \;+\; t_{346}\Delta y')\;; \quad (26)$$

c) and finally the term driven by the horizontal dispersion η_x and η'_x and orbit kick Δy and $\Delta y'$ via the second order matrix T:

$$\delta\,\langle yE\rangle \;=\; \frac{\sigma_E}{\sigma_{y0}}\,((t_{331}\Delta y \;+\; t_{341}\Delta y')\,\eta_x + \\ +(t_{332}\Delta y \;+\; t_{342}\Delta y')\,\eta'_x)\;. \quad (27)$$

Fig. 11 shows that the analytical results agree perfectly with tracking. Fig. 13 shows that contributions to the total effect can combine in a more or less favorable manner, depending on the sign of the dispersion with respect to the crossing angle, which is defined by the geometry of the Beam Delivery and the location of the detector. In particular, the reason why the vertical dispersion is smaller with the nominal crossing angle, as seen in Table I, is partial compensation of the horizontal dispersion and crossing angle terms.

For the case of zero crossing angle, it was shown above that a weak antisolenoid overlapping the FD can compensate both the $\langle yx'\rangle$ coupling and $\langle yE\rangle$ dispersion simultaneously. In this case, the condition for the combined detector solenoid and antisolenoid field to restore the solenoid cancellation at the IP, is to have

$$\int_{-\infty}^{0}\frac{B_z}{B\rho}\,(m_{12}m_{33} \;-\; m_{11}m_{34})\,dz \;=\; 0\;, \quad (28)$$

or, equivalently

$$\int_{-\infty}^{0}\frac{B_z}{B\rho}\,\frac{1}{\sqrt{\beta_x\beta_y}}\,(\alpha_y\beta_x S_X S_Y + \beta_x S_X C_Y - \beta_y S_Y C_X \\ -\alpha_x\beta_y S_X S_Y)\,dz \;=\; 0\;. \quad (29)$$

It is also clear that the conditions for cancellation of the solenoid effects do not depend on the optics parameters at the IP. For example, changing the IP β-function or angular dispersion η_0 would not affect the cancellation because they do not change the Final Doublet strength, which is defined to a major extent just by the geometry. Therefore, all matrix elements remain the same, and Equation 28 remains valid independent of the IP beam parameters.

In the case with a crossing angle, the cancellation conditions can be derived in a similar manner. In this case, it is less obvious from the analytical formulae that the cancellation of all terms can be achieved simultaneously. However, Fig. 11 indicates that this can be done, and it is demonstrated for the real detector model in the next section.

Finally, we include formulas for two other beam correlation terms which do not cancel even if the solenoid does not overlap the Final Doublet:

$$\langle yx\rangle \;=\; \frac{\sigma_{x0}}{\sigma_{y0}}\int_{-\infty}^{0}\frac{B_z}{2\,B\rho}\,(m_{21}m_{34} \;-\; m_{22}m_{33})\,dz\;, \quad (30)$$

and

$$\langle yy'\rangle \;=\; \frac{\sigma_{y'0}}{\sigma_{y0}}\int_{-\infty}^{0}\left(\frac{B_z}{2\,B\rho}\,m_{34}\right)^2 dz\;, \quad (31)$$

where the latter is proportional to the square of the field and just corresponds to solenoidal focusing. These terms

do not depend on θ_c, and they are usually much smaller than the other beam distortions considered above.

As noted above, the solenoid focusing was neglected in the presented consideration. Taking this focusing into account, it is easy to estimate that a short test solenoid placed in the final drift would result in the following residual offset at the IP:

$$\Delta y_{IP} \approx -\left(\frac{B\ell}{2\,B\rho}\right)^3 \frac{\theta_c\, Z_s^2}{\ell} \quad , \tag{32}$$

for $Z_s \gg \ell$. This would give about 0.024 nm if the above test solenoid is located at $Z_s = 3$ m. For the solenoid field that fills the final drift entirely, the estimate is

$$\Delta y_{IP} \approx -\left(\frac{B\ell}{2\,B\rho}\right)^3 \frac{\theta_c\, L_*}{3} \quad , \tag{33}$$

yielding about ten nanometers for a typical detector model at the nominal parameters, which is sufficiently small and does not affect the validity of formulas presented in this Section.

V. COMPENSATION OF IP BEAM SIZE USING WEAK ANTISOLENOIDS

The fields of the SiD with an optimized weak antisolenoid are shown in Fig. 14. The antisolenoid is placed on the detector axis, and its field is approximated by

$$B_{zAntisolenoid} = \frac{B_{z0}}{1 + ((z - z_0)/z_w)^4} \quad , \tag{34}$$

where the location $z_0 = 4.14$ m, width $z_w = 0.5$ m, and strength $B_{z0} = -1.5655$ T are optimized to cancel the beam offset at the IP and the two major beam distortions. The integral strength of this solenoid is 1.74 Tm.

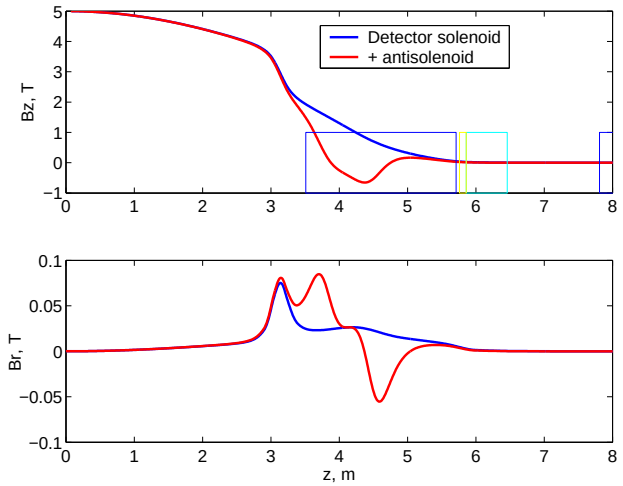

FIG. 14: Fields in SiD with and without the optimized weak antisolenoid.

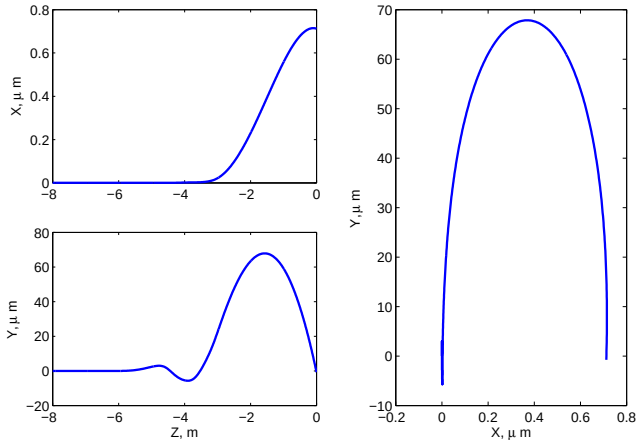

FIG. 15: Orbits with SiD fields compensated by a weak antisolenoid. IP is at $z = 0$ m.

The particular functional dependence of this approximation is irrelevant because the parameters can be easily reoptimized for calculated fields of realistic coils.

Orbits through the SiD with this antisolenoid are shown in Fig. 15. The IP vertical orbit offset is now canceled [21]. The beam phase space in SiD with this antisolenoid but without any other correcting knobs is shown in Fig. 16. The beam size is compensated to within 30%. Comparing with the bare SiD results given in Fig. 6 and Table I, it appears that this weak antisolenoid has compensated 99% of the effect.

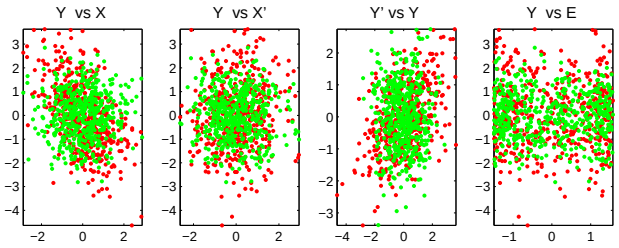

FIG. 16: Beam phase space in SiD with an antisolenoid but without any correction knobs. The beam size is $\sigma_x/\sigma_{x0} = 1.00$, $\sigma_y/\sigma_{y0} = 1.29$.

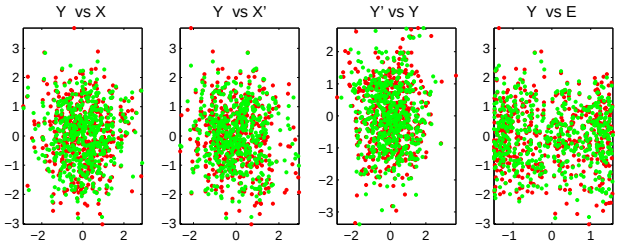

FIG. 17: Beam phase space in SiD with an antisolenoid and with additional correction knobs. The beam size is $\sigma_x/\sigma_{x0} = 1.00$, $\sigma_y/\sigma_{y0} = 1.003$.

The remaining deviation of the beam size from nominal is easy to correct with linear tuning knobs. These include BDS sextupole displacement knobs and skew quadrupole knobs in the skew correction section of the BDS, which allow orthogonal correction of the $\langle yE\rangle$, $\langle yy'\rangle$, $\langle yx\rangle$ and $\langle yx'\rangle$ terms, and similar terms in the horizontal plane, if necessary. The beam phase space in SiD with the antisolenoid, and with additional optimal linear knobs is shown in Fig. 17. One can see that the beam size is compensated to within 0.3% of nominal, which is within the resolution.

We have seen earlier in Table I and in Section IV, that with the bare SiD or LD solenoids, and with a positive crossing angle, the vertical dispersion term $\langle yE\rangle$ is rather small because the crossing angle term and the horizontal angular dispersion term approximately cancel each other. For a negative crossing angle, the $\langle yE\rangle$ term is doubled. However, this peculiar dependence on the crossing angle mostly disappears when the antisolenoid is used. Fig. 18 shows the dependence of the beam IP position and major beam distortions $\langle yx'\rangle$ and $\langle yE\rangle$ on the crossing angle, with and without the weak antisolenoid. The antisolenoid compensates the vertical IP position, coupling and vertical dispersion, and also eliminates most of the dependence on the crossing angle.

Agreement between analytical and tracking results shown in Fig. 18 is acceptable. A small difference of about 0.1 in the vertical dispersion term and several tens of nanometers in the vertical orbit is explained by the effect of the solenoid focusing, which was neglected in our analytic derivations. One can see that the assumption of the negligible solenoid focusing is indeed justified for our case, since these differences are small.

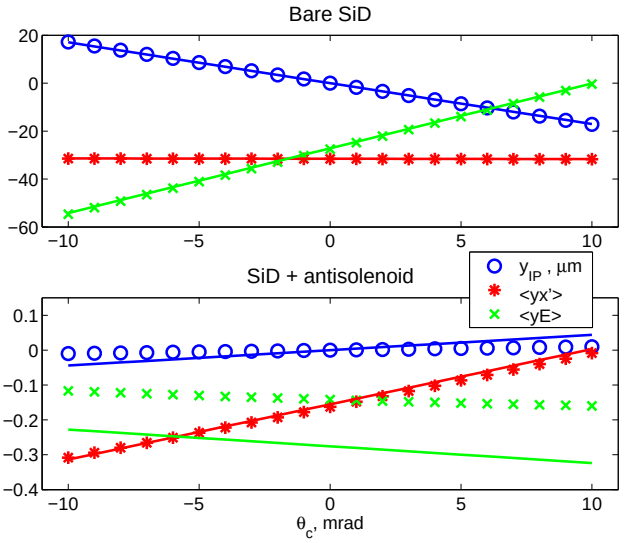

FIG. 18: Vertical orbit at the IP, and beam distortions $\langle yx'\rangle$ and $\langle yE\rangle$ in SiD without (top plot) and with antisolenoid (bottom plot) as a function of crossing angle. Symbols – tracking, lines – analytical results.

Regarding the technical implementation of the weak antisolenoid, it is essential that this antisolenoid is aligned on the detector axis, so it should be built as an integral part of the SiD detector. The antisolenoid should have at least two coils, separated longitudinally and individually powered, in order to provide fine adjustment of both the amplitude and longitudinal position of the antisolenoid field. It should be compact, to minimize interference and space taken from the detector, and should be able to withstand the longitudinal forces acting on the antisolenoid due to the main solenoid field (these forces prohibit the use of an antisolenoid wound on QD0 quadrupole and placed on the beam axis).

The use of antisolenoids to shielding the final quadrupole was considered by the GLC project [19], but their purpose was to protect the iron electromagnetic quadrupole from saturation in the solenoid field and not for beam size compensation. The design of this solenoid can be modified to also provide beam size compensation. In this case, the iron of the quadrupole would also shield part of the solenoid field, helping the compensation, but any remaining field beyond the first quadrupole in the FD would also need to be compensated.

The antisolenoids optimized for the LD case are shown in Fig. 19. Here the field extends much farther into the FD, and though there might be a solution with a single antisolenoid, two antisolenoids appear to be effective.

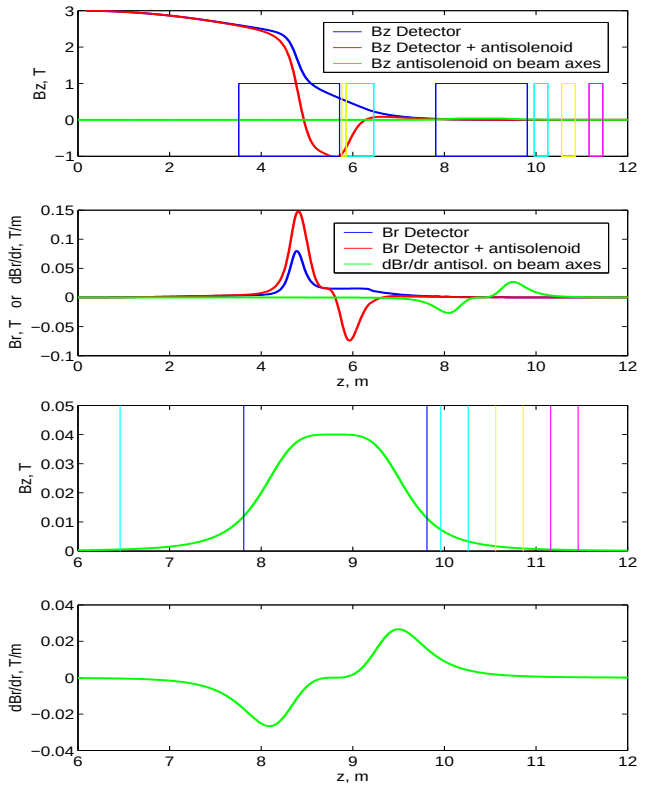

FIG. 19: Fields in LD with optimized antisolenoids. The two bottom plots zoom into the region of the second antisolenoid.

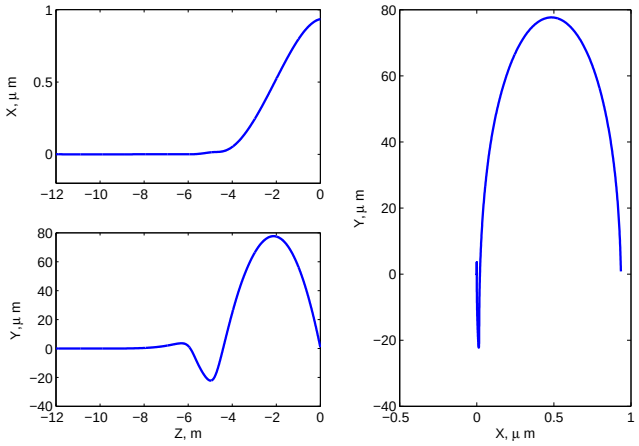

FIG. 20: Orbits in LD with antisolenoids.

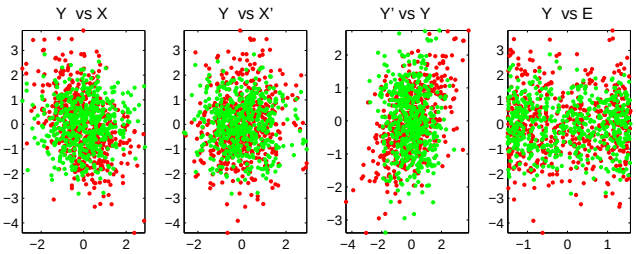

FIG. 21: Beam phase space in LD with antisolenoids, but without any correction knobs. The beam size is $\sigma_x/\sigma_{x0} = 1.00$, $\sigma_y/\sigma_{y0} = 1.23$.

The first is on the detector axis, overlapping with part of QD0 ($z_0 = 5.4$ m , $z_w = 0.6$ m, $B_{z0} = -1.699$ T, the integral strength 2.26 Tm), and the second is on the beam axis, overlapping with QF1 ($z_0 = 8.8$ m , $z_w = 0.8$ m, $B_{z0} = 0.04$ T, the integral strength 0.071 Tm). This second solenoid could actually be wound on QF1 (provided QF1 is not an iron quadrupole) since the forces from the main solenoid are already very small. The second solenoid gives additional flexibility to correct all the beam correlations, in spite of the fact that it is very weak.

The orbit in LD with these antisolenoids is shown in Fig. 20. Again, the IP vertical offset is canceled. The beam phase space in LD with antisolenoids but without any correction knobs is shown in Fig. 21. The beam size is compensated within 23% of nominal. Thus the weak antisolenoids have compensated 99.8% of the effect. The beam phase space in LD with antisolenoids and with additional linear knobs to correct the remaining effects is shown in Fig. 22. The beam size is compensated within 0.9% of nominal.

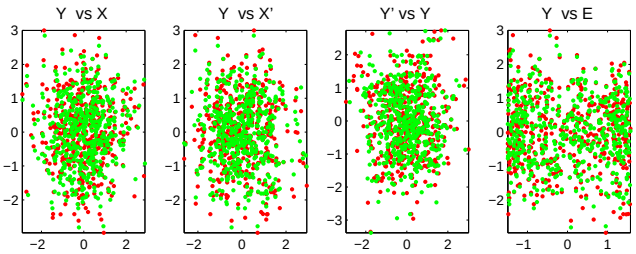

FIG. 22: Beam phase space in LD with antisolenoids and with additional linear knobs. The beam size is $\sigma_x/\sigma_{x0} = 1.00$, $\sigma_y/\sigma_{y0} = 1.009$.

Compensation with weak antisolenoids appears quite effective. The integrated strength of these antisolenoids is only 10–15% of the SiD or LD integrated strength, so they can be made compact to minimize interference with the detector, yet they cancel more than 99% of the effect of the detector solenoid. The remaining beam distortions are sufficiently small to be easily corrected with the linear tuning knobs of the BDS.

To maximize physics capabilities, the detector should operate with the same solenoid field for any beam energy in the range of the collider. For the first stage of NLC operation, this spans from 50 to 350 GeV, with a nominal beam energy of 250 GeV. Thus, it is important to characterize the performance of the beam size compensation over the full range of energies. As the beam energy decreases, the solenoid effect on the beam size increases at least linearly, and for certain terms quadratically (such as $\langle yy' \rangle$, see Eq. 31).

The effect of the SiD solenoid on the IP beam size as a function of energy is shown in Fig. 23 (top plot). The beam size at 50 GeV increases to more than a hundred times nominal (the nominal beam size depends on energy as $1/\sqrt{E}$). The dominant beam distortions are $\langle yx' \rangle$ coupling, and the second largest term at low energy is $\langle yy' \rangle$ focusing.

An advantage of weak antisolenoids is that they can-

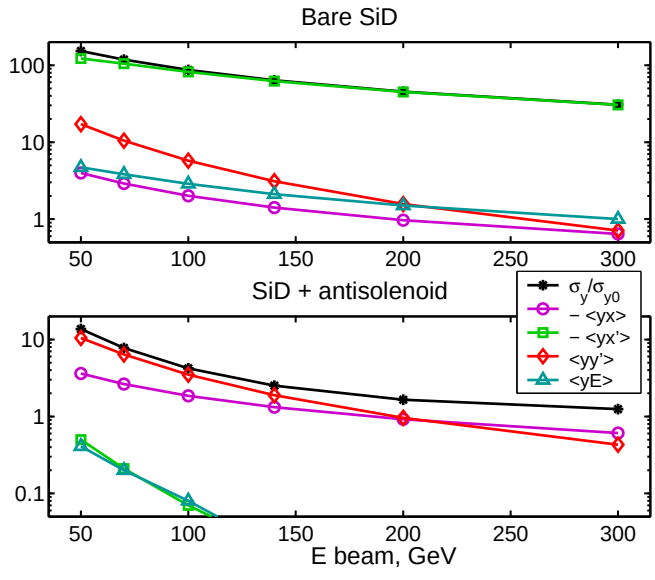

FIG. 23: Beam size and beam distortions in SiD, as a function of beam energy without and with antisolenoid. Linear correction knobs have not been applied.

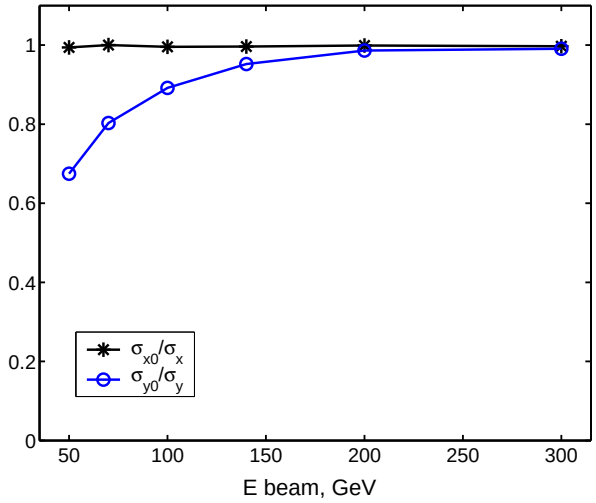

FIG. 24: Beam size in SiD with the antisolenoid as a function of beam energy. The beam size is corrected *only with linear knobs*.

cel the effect of the main detector solenoid almost completely, and the major terms are canceled for any beam energy. Fig. 23 (bottom plot) shows the IP beam size and distortions for the SiD with the antisolenoid. The antisolenoid compensates more than 99% of the solenoid effect at 300 GeV and more than 90% at 50 GeV.

For SiD plus antisolenoid, the remaining linear distortions can be corrected by linear knobs. At the lowest beam energy, the quadrupoles QD0 and QF1 were adjusted to compensate the solenoid focusing term $\langle yy' \rangle$, skew quadrupoles in the skew correction section were used to correct the $\langle yx \rangle$ term, and sextupole displacement knobs were used for fine adjustment of $\langle yE \rangle$, $\langle xE \rangle$

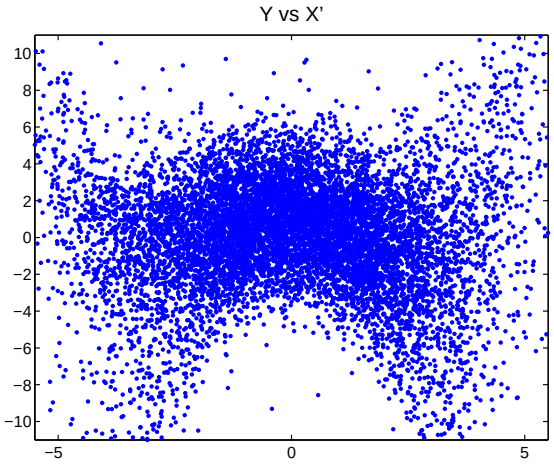

FIG. 25: The $(y - x')$ beam phase space at the IP for the LD with the antisolenoids at 50 GeV, corrected *only with linear knobs*, showing the remaining second order term $\langle yx'x' \rangle$ and higher order distortions.

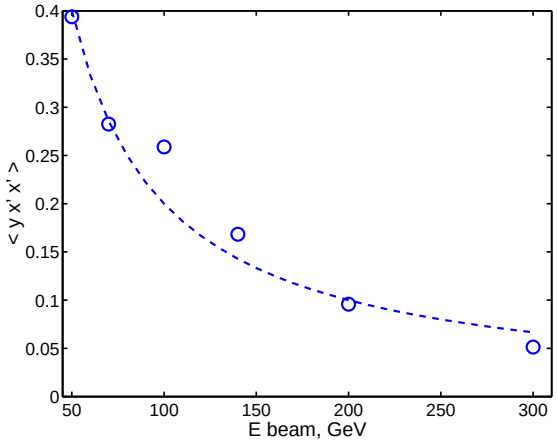

FIG. 26: One of the remaining second order terms at the IP, $\langle yx'x' \rangle$, for the SiD model with an antisolenoid corrected *only with linear knobs*.

and $\langle yx' \rangle$. The beam size at the IP is shown in Fig. 24 for SiD plus antisolenoid and corrected using only these knobs. The beam size correction is better than 10% down to 100GeV/beam, and within 35% at 50 GeV. The remaining increase of the beam size is due to higher order distortions, in particular, the second order coupling term $\langle yx'x' \rangle$ shown in Fig. 25 and Fig. 26, which arise because the linear knobs such as $\langle yx \rangle$ needed at low energy are too strong.

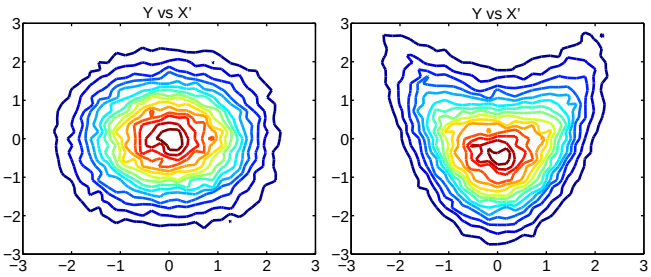

FIG. 27: Illustration of second order knob acting on $\langle yx'x' \rangle$, involving rotation of sextupoles. Left – nominal beam, right – distorted beam with $\langle yx'x' \rangle \approx 0.8$, obtained with tracking.

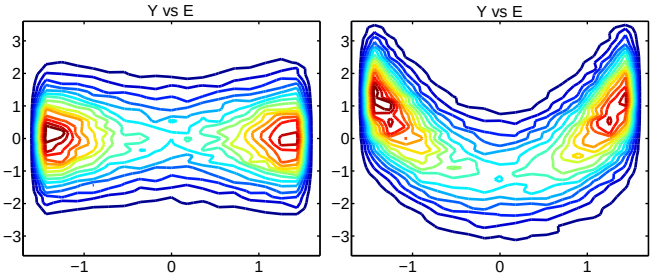

FIG. 28: Illustration of second order knob acting on $\langle yEE \rangle$, involving rotation of sextupoles. Left – nominal beam, right – distorted beam with $\langle yEE \rangle \approx 0.6$, obtained with tracking. Note that the nominal beam has a non-Gaussian two-horn "Batman" distribution in energy.

Further correction of the beam size at low energy requires tuning with higher order knobs. A discussion of this procedure is beyond the scope of this paper and can be found in [20]. For illustration, Fig. 27 and Fig. 28 show the results of second order knobs acting on $\langle yx'x'\rangle$ and $\langle yEE\rangle$ beam distortions. These particular knobs require rotation of the BDS sextupoles. Other second order knobs also adjust the sextupole strength.

The performance of solenoid compensation using weak antisolenoids can be compared with compensation using skew quadrupoles in the FD, for the SiD detector. The best results with skew quadrupoles were obtained not with the skew quadrupole SQ3 located next to the FD, but with a rotation of QD0, which gives a more local correction of the $\langle yx'\rangle$ coupling.

Using only the quadrupole rotation, the IP vertical orbit is not compensated naturally. To restore the orbit requires offsets of QD0 and QF1 and an additional dipole corrector (BXCOR in Fig.2) located between 6.6 and 7.6 m in the FD. These three dipole correctors cancel both the vertical dispersion and vertical offset at the IP, without introducing a second order vertical dispersion.

The rest of the distortions were compensated as for the antisolenoid case, adjusting the QD0 and QF1 strength to correct $\langle yy'\rangle$, and the BDS skew correction to cancel $\langle yx\rangle$. Using the QD0 rotation and these linear knobs, the vertical beam size was corrected to $\sigma_y/\sigma_{y0} = 1.71$ at 50 GeV, in comparison with the $\sigma_y/\sigma_{y0} = 1.48$ that was achieved with the antisolenoid.

This suggests that, though the weak antisolenoid correction gives better performance, the skew quadrupole method may also be feasible, although it would require more sophisticated linear and higher order tuning. However, one of the disadvantages of the rotated quadrupole method is that changing the beam energy would require either mechanical rotation of QD0 or adjustment of its skew winding, if it is superconducting.

In the case of the weak antisolenoids, the fact that the compensation is independent of beam energy is an advantage that would significantly ease operation of the machine.

Finally, the effect of the crab-cavity on the solenoid compensation and beam size at IP has been investigated and found negligible. This cavity is located about 12 m from the IP, and produces a horizontal kick on the beam correlated with the longitudinal position within the bunch. As a result, the beam at the IP becomes tilted in $x - z$ plane by the angle θ_c, providing the nominal head-on collision with the opposite beam. Due to the detector solenoid coupling, the crab-cavity kick would also cause a $y - z$ tilt at IP which is easily corrected by rotation of the crab-cavity about the longitudinal axis. Once this (energy dependent) correction is made, the effect of the crab cavity on the beam size vanishes.

VI. CONCLUSION

The solenoid field of the Linear Collider experimental detector will distort the beam size at the Interaction Point unless compensated. This paper discusses the optics effects and the performance of various methods of compensation. Most of the effect on the beam size is caused by the part of the solenoid field which overlaps and extends beyond the final focusing quadrupoles. The most efficient and most local compensation is achieved with weak antisolenoids near the IP. A compensation scheme using only skew quadrupoles is less efficient but also feasible. An important advantage of the antisolenoid is that the compensation is effective over the entire NLC beam energy range.

VII. ACKNOWLEDGEMENT

The authors thank John Hodgson for providing ANSYS models of the NLC detectors, Peter Tenenbaum for developing the DIMAD models of BDS with overlapping solenoid field, Brett Parker, Nan Phinney and Tor Raubenheimer for very useful discussions. The work was supported by the U.S. Department of Energy, Contract Number DE-AC03-76SF00515.

[1] J.J. Murray, "A General Method, a la TRANSPORT, for Evaluation of the Perturbing Effects of Solenoidal Inserts in Storage Ring Interaction regions," SLAC Note PEP-219, July 1976.

[2] KEKB B-Factory Design Report, KEK Report 95-7, 1995.

[3] M. Bassetti, M.E. Biagini, C. Biscari, "Solenoidal Field Compensation," Proc. Advanced ICFA Beam Dynamics Workshop, p. 209, Frascati, Italy, October 1997.

[4] LEP Design Report, Vol. 2, CERN-LEP-84-01, June 1984.

[5] Y. Nosochkov, Y. Cai, J. Irwin, M. Sullivan, E. Forest, "Detector Solenoid Compensation in the PEP-II B-Factory," Proc. 1995 Part. Acc. Conf., p.585, Dallas, May 1995.

[6] A. Seryi, Y. Nosochkov, M. Woodley, "Beam Delivery Layout For The Next Linear Collider", Proc. 2004 European Part. Acc. Conf., Lucerne, July 2004.

[7] Pantaleo Raimondi and Andrei Seryi, "A Novel Final Focus Design For Future Linear Colliders", SLAC-PUB-8460, May 2000; Phys. Rev. Lett. 86:3779-3782, 2001.

[8] R. Talman, "Single Particle Motion," Proc. Lecture Notes in Physics, 343, p. 42, Capri, Italy, 1989.

[9] J.J. Murray, "Skew Quad Compensation at PEP," SLAC Note PEP-256, October 1977.

[10] S. Peggs, "The Projection Approach to Solenoid Com-

pensation," CERN/SPS/82-2 (DI/MST), January 1982.
[11] R. H. Helm, "Adiabatic Approximation For Dynamics Of A Particle In The Field Of A Tapered Solenoid," SLAC-0004, Aug 1962.
[12] P. Tenenbaum, J. Irwin, T.O. Raubenheimer, "Beam Dynamics of the Interaction Region Solenoid in a Linear Collider due to a Crossing Angle", Phys. Rev. Spec. Topics – Acc. and Beams, v. 6, 061001 (2003).
[13] A. Wolski, "Compensation of Solenoid Effects at the TESLA Interaction Point," TESLA Report 2000-13, July 2000.
[14] J.J. Murray, "Effects of Superposition of Detector Solenoid and FFS Quadrupole Fields in SLC and Correction Methods," SLAC-CN-237, July 1983.
[15] TESLA Final Focus System With Superconducting Magnets In The Interaction Region: Optics, Tolerances And Magnet Design. By Olivier Napoly, Etienne Klein, Jean Michel Rifflet (DAPNIA, Saclay),. DAPNIA-94-10, Oct 1994. 33pp. Contribution to TESLA Workshop '94, Frascati, Italy, 8-10 Nov 1994.
[16] Peter Tenenbaum, "New Beam Delivery System Optics: BDS9901", LCC-Note-020, July 1999.
[17] Roger Servranckx, Karl Brown, Lindsay Schachinger, David Douglas, Peter Tenenbaum, "Users Guide To The Program DIMAD", SLAC-285, Jan 1990, and also the latest version of the Users guide, January 4, 2004, http://www.slac.stanford.edu/accel/nlc/local/AccelPhysics/codes/dimad/dimad.pdf
[18] Brett Parker and Andrei Seryi, "Compensation of the Effects of Detector Solenoid on the Vertical Beam Orbit in NLC", LCC-Note-143, SLAC-TN-04-044, June 2004.
[19] "GLC Project", KEK Report 2003-7, September 2003.
[20] Y. Nosochkov, P. Raimondi, T.O. Raubenheimer, A. Seryi, M. Woodley, "Tuning Knobs For The NLC Final Focus", SLAC-PUB-9255, Jun 2002, in Proc. EPAC 2002, Paris, France, 3-7 Jun 2002.
[21] The small nonzero horizontal offset at the IP can be easily corrected, and the vertical angle is of no concern for luminosity, since in e+e- collider the orbits will be antisymmetrical, and the beams will still collide head-on. For the e-e- version of the collider, or if more careful preservation of the beam polarization is needed, the vertical angle at the IP can also be locally compensated using the so called Detector Integrated Dipole (DID) corrector, as suggested in [18], which is compatible with the beam size compensation using weak antisolenoids.